Monthly Notices of the ROYAL ASTRONOMICAL SOCIETY

MNRAS **444,** 2544–2554 (2014) doi:10.1093/mnras/stu1670

Collisional excitation of singly deuterated ammonia NH_2D by H_2

F. Daniel,[1]★ A. Faure,[1] L. Wiesenfeld,[1] E. Roueff,[2] D. C. Lis[3,4] and P. Hily-Blant[1]

[1]*IPAG, Observatoire de Grenoble, Université Joseph Fourier, CNRS UMR5571, B.P. 53, F-38041 Grenoble Cedex 09, France*
[2]*LERMA and UMR 8112, Observatoire de Paris, Place J. Janssen, F-92190 Meudon, France*
[3]*Sorbonne Universités, Université Pierre et Marie Curie, Paris 6, CNRS, Observatoire de Paris, UMR 8112, LERMA, F-75014 Paris, France*
[4]*California Institute of Technology, Cahill Center for Astronomy and Astrophysics 301-17, Pasadena, CA 91125, USA*

Accepted 2014 August 13. Received 2014 July 22

ABSTRACT

The availability of collisional rate coefficients with H_2 is a pre-requisite for interpretation of observations of molecules whose energy levels are populated under non-local thermodynamical equilibrium conditions. In the current study, we present collisional rate coefficients for the NH_2D/para-H_2($J_2 = 0$, 2) collisional system, for energy levels up to $J_\tau = 7_7$ ($E_u \sim 735$ K) and for gas temperatures in the range $T = 5$–300 K. The cross-sections are obtained using the essentially exact close-coupling (CC) formalism at low energy and at the highest energies, we used the coupled-states (CS) approximation. For the energy levels up to $J_\tau = 4_2$ ($E_u \sim 215$ K), the cross-sections obtained through the CS formalism are scaled according to a few CC reference points. These reference points are subsequently used to estimate the accuracy of the rate coefficients for higher levels, which is mainly limited by the use of the CS formalism. Considering the current potential energy surface, the rate coefficients are thus expected to be accurate to within 5 per cent for the levels below $J_\tau = 4_2$, while we estimate an accuracy of 30 per cent for higher levels.

Key words: molecular data – molecular processes – scattering.

1 INTRODUCTION

Singly deuterated ammonia, NH_2D, was first tentatively detected towards the Kleinmann-Low (KL) nebula in Orion (Rodriguez Kuiper, Kuiper & Zuckerman 1978) and towards Sgr B2 (Turner et al. 1978). However, due to the molecular richness of these objects, a blending with transitions from other molecular species could not be discarded at that time. The first unambiguous detection of NH_2D was subsequently performed by Olberg et al. (1985) in the cold environment of L183, S140 and DR21(OH) at 85 and 110 GHz, thanks to the high-spectral resolution of the observations which enabled them to resolve the hyperfine structure of the lines. Since then, its centimetre and millimetre rotational transitions have been used as tracers of the physical conditions and chemistry of the molecular gas over a wide range of conditions, ranging from cold prestellar cores (e.g. Saito et al. 2000; Tiné et al. 2000; Shah & Wootten 2001; Hatchell 2003; Roueff et al. 2005; Busquet et al. 2010) to warm star-forming regions (e.g. Walmsley et al. 1987; Pillai et al. 2007). In cold environments, the deuterium fractionation was derived to be several 10^{-2}. Such high fractionation ratios are within the values predicted by gas-phase models at low temperatures (Roueff et al. 2005). In warm environments such as Orion KL, the fractionation ratio was derived to be 0.003 by Walmsley et al. (1987) and interpreted as a possible signature of mantle evaporation. More recently, NH_2D has been detected at much higher frequencies thanks to *Herschel*. In Orion KL (Neill et al. 2013), several excited levels of NH_2D up to $J_{K_a,K_c} = 7_{5,3}$ ($E_u \sim 600$ K)[1] were detected and the fractionation ratio was derived to be 0.0068. The temperature and density associated with the emitting regions were estimated to $T \sim 100$–300 K and n (H_2) $\sim 10^7$–10^8 cm^{-3}.

In order to interpret the NH_2D observations, a key ingredient of the modelling is the collisional rate coefficients. Before the current calculations, the only available rate coefficients considered He as a collisional partner (Machin & Roueff 2006). However, it was shown in the case of ND_2H that the rate coefficients with He and H_2 can differ by factors of 3–30, depending on the transition (Machin & Roueff 2007; Wiesenfeld et al. 2011). Thus, a dedicated calculation for NH_2D with H_2 is required in order to interpret the observations of this molecule. Indeed, as discussed by Daniel et al. (2013), a simple scaling of the NH_2D/He rate coefficients is insufficient to accurately model the observations, at least under cold dark clouds conditions.

[1] NH_2D is an asymmetric top whose rotational energy structure can be described with the J, K_a, K_c quantum numbers. Alternatively, one may use the pseudo quantum number $\tau = K_a - K_c$. In what follows, we mainly use the J_τ notation to describe the rotational energy levels but can alternatively make use of the J_{K_a,K_c} notation, which is usually employed in astrophysical studies.

★ E-mail: fabien.daniel@obs.ujf-grenoble.fr

This paper is organized as follows. The potential energy surface (PES) is described in Section 2 and the collisional dynamics based on this surface in Section 3. We then describe the rate coefficients in Section 4 with some emphasis placed on their expected accuracy. In Section 5, we discuss the current results with respect to other related collisional systems and finally, we present conclusions in Section 6.

2 POTENTIAL ENERGY SURFACE

The rigid-rotor NH_2D–H_2 PES was derived from the NH_3–H_2 PES computed by Maret et al. (2009), but in the principal inertia axes of NH_2D. The scattering equations to be solved (see below) are indeed written for a PES described in the frame of the target molecule, here NH_2D. In the original NH_3–H_2 PES, the ammonia and hydrogen molecules were both assumed to be rigid, which is justified at temperatures lower than ∼1000 K. The NH_3 and H_2 geometries were taken at their ground-state average values, as recommended by Faure et al. (2005) in the case of the H_2O–H_2 system. The rigid-rotor NH_3–H_2 PES was computed at the coupled-cluster CCSD(T) level with a basis set extrapolation procedure, as described in Maret et al. (2009) where full details can be found. In the present work, the geometry of NH_2D was assumed to be identical to that of NH_3, i.e. the effect of deuterium substitution on the ammonia geometry was neglected. This assumption was previously adopted for the similar ND_2H–H_2 system by Wiesenfeld et al. (2011). We note that internal geometry effects are indeed expected to be only moderate ($\lesssim$30 per cent) at the temperatures investigated here, as shown by Scribano, Faure & Wiesenfeld (2010) for the D_2O–H_2 system. The main impact of the isotopic substitution on the NH_3–H_2 PES is therefore the rotation of the principal inertia axes.

We have thus expressed the NH_3–H_2 PES of Maret et al. (2009) in the principal inertia axes of NH_2D. The transformation can be found in Wiesenfeld et al. (2011, equations 2 and 3), where the γ angle is equal to -8.57 deg for NH_2D, as determined experimentally by Cohen & Pickett (1982). The shift of the centre of mass was also taken into account: the coordinates of the NH_2D centre of mass in the NH_3–H_2 reference frame were found to be $X_{CM} = 0.101\,312$ Bohr and $Y_{CM} = -0.032\,810$ Bohr, where X_{CM} and Y_{CM} were calculated for the ground-state average geometry of NH_3 used by Maret et al. (2009). The NH_2D–H_2 PES was generated on a grid of 87 000 points consisting of 3000 random angular configurations combined with 29 intermolecular distances in the range 3–15 Bohr. This PES was finally expanded in products of spherical harmonics and rotation matrices, as in Wiesenfeld et al. (2011, see their equation 4), using a linear least-squares fit procedure. We selected iteratively all statistical significant terms using the procedure of Rist & Faure (2011) applied at all intermolecular distances. The final expansion included anisotropies up to $l_1 = 10$ for NH_2D and $l_2 = 4$ for H_2, resulting in a total of 210 angular basis functions. The root-mean-square residual was found to be lower than 1 cm^{-1} for intermonomer separations R larger than 5 Bohr, with a corresponding mean error on the expansion coefficients smaller than 1 cm^{-1}.

3 COLLISIONAL DYNAMICS

In order to describe the NH_2D energy structure, we adopted the same approach as used by Machin & Roueff (2006), i.e. we assumed that NH_2D is a rigid rotor and we neglected the inversion motion corresponding to the tunnelling of the nitrogen atom through the H_2D plane. The spectroscopic constants, adapted from the CDMS catalogue (Müller et al. 2001) and from Coudert, Valentin & Henry (1986), are given in table 2 of Machin & Roueff (2006). As outlined in Machin & Roueff (2006), neglecting the inversion motion leads to neglecting the difference between the ortho and para states of NH_2D, which are thus treated as degenerate. Indeed, by considering the inversion motion, every rotational state would be split into two states which are either symmetric or antisymmetric under exchange of the protons. By combining the symmetry of each state with the symmetry of the nuclear wavefunctions, each state will either correspond to an ortho or para state to ensure that the overall wavefunction is antisymmetric under the exchange operation. Since the collisional transitions are only possible within a given symmetry, the treatment of the collisional dynamics would be essentially similar for each species, except for the slight differences of energy between the ortho and para states, which is of the order of ∼0.4 cm^{-1} independently of the rotational state (Coudert & Roueff 2006). Hence, by neglecting the inversion motion, we obtain a set of rate coefficients which applies to both the ortho and para symmetries of NH_2D. Finally, we also considered H_2 as a rigid rotor and adopted a rotational constant of 59.2817 cm^{-1} (Huber & Herzberg 1979). The reduced mass of the collisional system is $\mu = 1.812\,998\,990$ a.m.u.

In order to solve the collisional dynamics, we used the MOLSCAT code.[2] Since NH_2D is observed in warm media and since the transitions detected include levels up to $J = 7$, our goal was set accordingly. We performed the calculations in order to provide rate coefficients for the NH_2D energy levels up to $J_\tau = 7_7$ and for the temperature range $T = 5$–300 K. A first step consisted of adjusting the convergence of the dynamical calculations for these levels and for total energies up to $E_t \sim 3000$ cm^{-1}. We thus performed a few calculations at some specific values of the total energy for which we determined the number of NH_2D rotational energy levels, as well as the integration step required to ensure a convergence better than 1 per cent below 530 cm^{-1} and better than 5 per cent above this threshold. These test calculations are summarized in Fig. 1, and the parameters used for each energy range are also indicated. We found that including the $J_2 = 2$ level of para-H_2 in the dynamical calculations had a large impact on the resulting cross-sections. Indeed, at some specific energies, we found that the cross-sections obtained with the $J_2 = 0$ or $J_2 = 0$, 2 basis can differ by up to a factor of 7. An example of the influence of the $J_2 = 2$ energy level of H_2 on the cross-sections is given in Fig. 2. This figure will be further discussed below.

At low total energy (i.e. $E_t < 110$ cm^{-1}), we performed dynamical calculations with the accurate close-coupling (CC) formalism. However, because of the increase of the computational time with the number of channels, the cost in terms of CPU time became prohibitive at high energy. As an example, in the range 100–110 cm^{-1}, the CPU time typically ranged from 40 to 90 h per energy, the amount of time being dependent on how far the energy is from the last opened energy level. In order to keep the CPU time spent within a reasonable amount of time, we had two options. We could either increase the step between two consecutive energy grid points or switch to an approximate method in order to solve the collisional dynamics. While the first option could be a good choice for the low-lying energy levels, it would turn to be a bad choice for the highest ones, since our calculations show that typically that the cross-sections have resonances for kinetic energies up to ∼150 cm^{-1}

[2] J. M. Hutson and S. Green, MOLSCAT computer code, version 14 (1994), distributed by Collaborative Computational Project No. 6 of the Engineering and Physical Sciences Research Council (UK).

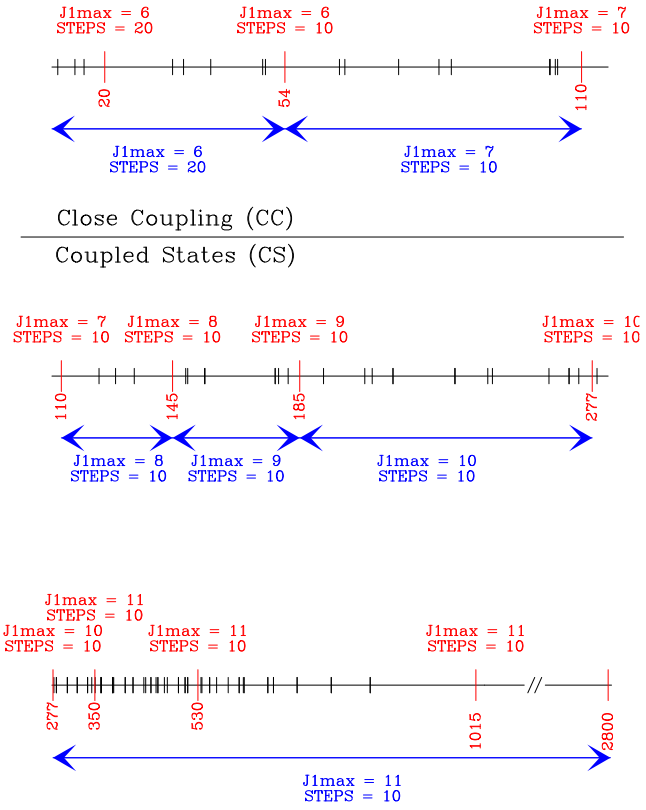

Figure 1. Parameters that describe the convergence of the dynamical calculations performed with MOLSCAT. J1max stands for the maximum quantum number of NH_2D, and STEPS is inversely proportional to the integration steps of the propagator. In red, we indicate the total energies at which we checked for the convergence of these two parameters. In blue, we indicate the values used for each energy range. Additionally, we also reported the energy levels of NH_2D which appear as vertical lines.

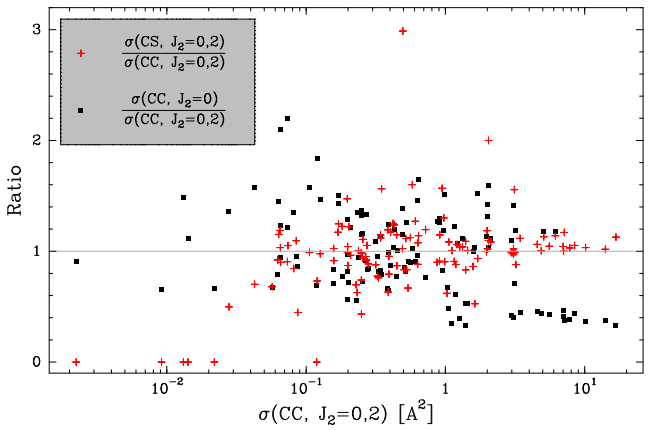

Figure 2. Ratio at 110 cm^{-1} between two approximate sets of cross-sections with respect to CC cross-sections obtained with a $J_2 = 0, 2$ basis of H_2. The first approximate set (red crosses) corresponds to cross-sections obtained with the CS formalism and with a $J_2 = 0, 2$ basis of H_2. The second set (black points) is obtained with the CC formalism but the basis of H_2 is reduced to $J_2 = 0$.

above the threshold of the transition. Thus, because the NH_2D energy levels are close in energy, and because we are interested in the levels up to $J_\tau = 7_7$ ($E \sim 512$ cm^{-1}), an accurate description of the resonances for all the transitions requires the step between consecutive energies to be low (i.e. typically of 0.2 cm^{-1}) up to a total energy of ∼660 cm^{-1}. Therefore, we made the choice to use an approximate method to solve the dynamics. We considered two options: reducing the basis of H_2 still using the CC formalism or using the coupled-states (CS) formalism (McGuire & Kouri 1974) with the $J_2 = 0$, 2 basis for H_2. In Fig. 2, we show the ratio of the cross-sections obtained with those two treatments with respect to the cross-sections obtained with the CC formalism and with the $J_2 = 0, 2$ basis for H_2. In this example, the total energy is 110 cm^{-1} but we checked that the conclusions are similar at other values. Considering this figure, it appears that the CS method gives a fairly accurate description of the dynamics, especially for the transitions with the highest cross-sections. Indeed, it can be seen that for the transitions with cross-sections higher than 2 $Å^2$, the CS method is accurate within a factor of ∼1.2 for most transitions. On the other hand, reducing the basis of the H_2 molecule with the CC formalism introduces larger errors, up to a factor of ∼3 in this case. We thus made the choice to use the CS approximation to perform the dynamical calculations above 110 cm^{-1}, since the reduced amount of computational time (typically reduced by a factor of 10–20) enables us to adopt a fine energy grid. The step between consecutive energies is given in Table 1. In order to emphasize on the necessity to resort to an approximate method to perform the dynamical calculations, we note that the total CPU time spent to obtain the rate coefficients was ∼170 000 h (∼19 yr), a time however substantially reduced by the availability of a cluster of cores (336 cores of 2.26 GHz). Finally, in order to obtain a set of rate coefficients as accurate as possible, we scaled the CS cross-sections by performing a few calculations with the CC formalism, up to total energies of 250 cm^{-1}. These calculations enable to scale the transitions that involve the levels up to $J_\tau = 4_2$, and the procedure used to perform the scaling is described in Appendix A. The scaled and original CS cross-sections are reported in Fig. 3 for a few transitions. Note that as expected from formal criteria (see Heil, Kouri & Green 1978, and references therein), we observe that the accuracy of the CS formalism increases with the kinetic energy.

Table 1. Step between the consecutive total energies used to characterize the cross-sections.

Energy range (cm^{-1})	Step in energy (cm^{-1})
< 110	0.1
110–277	0.2
277–630	0.5
630–690	2
690–755	4
755–1355	20
1355–2800	50

Apart from its accuracy, the CS formalism has the additional drawback that some transitions are predicted to be null while they should not be, which is a consequence of the neglect of small coupling terms. This can be seen in Fig. 2 where a few transitions below 0.2 $Å^2$ have ratios equal to zero. The transitions which are predicted to be null with the CS formalism correspond to $J_\tau \rightarrow 0_0$, where τ ranges from $\tau = -J + 1$ to $\tau = J - 1$ in a step of 2. The transitions concerned correspond to H_2 transitions with $J_2 = 0 \rightarrow 0$. In Fig. 4, we report the de-excitation transitions connected to the 0_0 level for the levels up to $J_\tau = 4_4$. For the transitions with non-null CS cross-sections (indicated in red in Fig. 2), the values reported correspond to the CC and scaled CS cross-sections. For

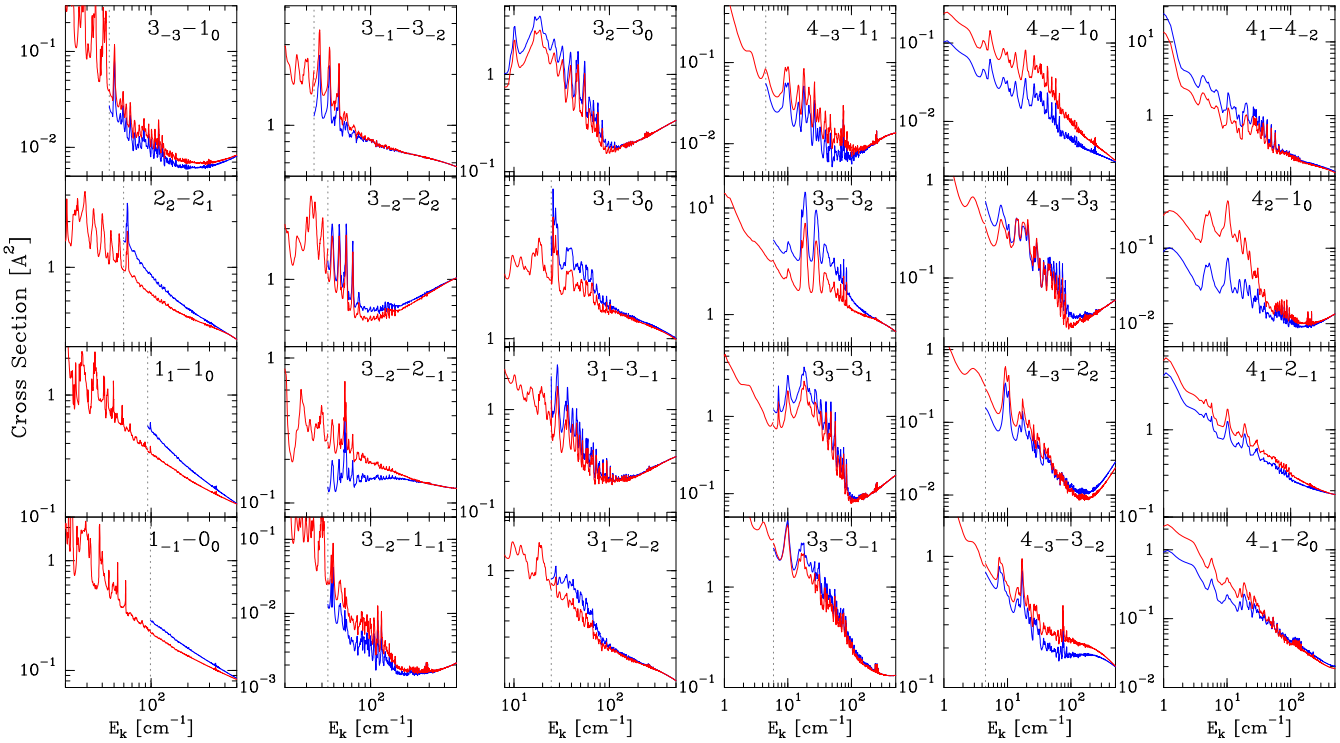

Figure 3. Cross-sections as a function of the kinetic energy E_k. The blue curve corresponds to the CS calculations. The red curve corresponds to the CC calculations, below a total energy of 110 cm^{-1} and to the scaled CS calculations above this threshold. The correspondence between this particular value of the total energy and the kinetic energy is indicated for each transition by a dotted vertical line.

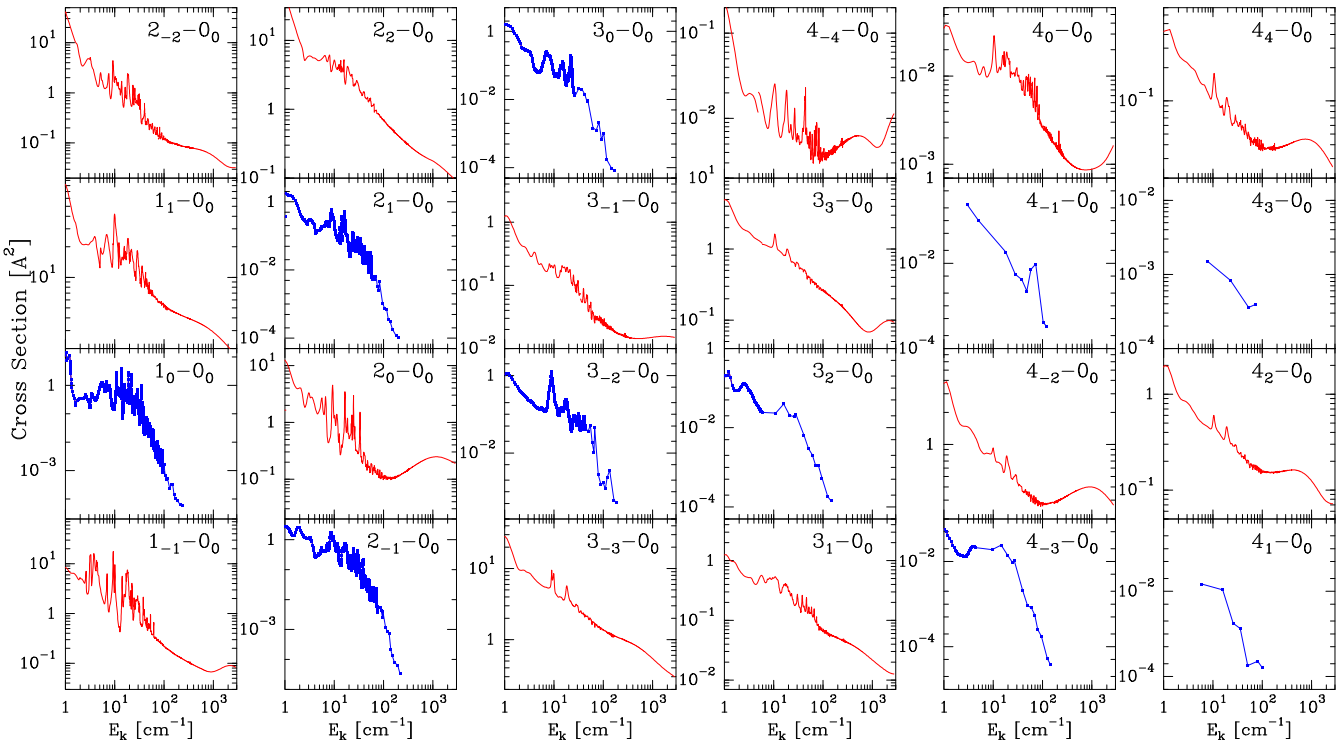

Figure 4. Cross-sections for the transitions connected to the fundamental energy level and for levels up to $J_\tau = 4_4$. The red curves correspond to CC plus scaled CS cross-sections. The blue curves correspond to CC calculations and are truncated in energy since the CS formalism predicts null cross-sections.

the other transitions (indicated in blue), we report the CC points we calculated. For the latter, we included the reference CC points used to scale the CS cross-sections, i.e. for total energies between 110 and 250 cm^{-1}, which explains why the step in energy is large for the highest kinetic energies. First, when considering this figure, it is important to notice that the cross-sections predicted to be null with the CS formalism are indeed of lower magnitude by comparison with other transitions. Additionally, from the few transitions available, it appears that these cross-sections decrease quickly with increasing kinetic energy. As an example, the $1_0 \rightarrow 0_0$ transition decreases by four orders of magnitude between 1 and 110 cm^{-1}. Finally, all these transitions seem to share a similar shape. These peculiarities of the null CS cross-sections make it possible to calculate the rate coefficients for the levels up to $J_\tau = 3_2$, with a reasonable accuracy up to 300 K, despite the truncation in energy of the grid. This point will be further discussed in the next section where we also derive analytical formulae which are used to estimate the null $J_\tau \rightarrow 0_0$ rate coefficients for the levels above $J_\tau = 3_2$.

Finally, since we performed calculations with a $J_2 = 0, 2$ basis for H_2 and since the energy grid was well sampled, the cross-sections that involve the excited $J_2 = 2$ state of H_2 can be used to derive the corresponding rate coefficients. Indeed, the convergence criteria previously discussed also apply to the $J_2 \rightarrow J_2'$ transitions with either J_2 or J_2' equal to 2. In Fig. 5, we give a characteristic example of such transitions and show the transitions related to the $2_{-2} \rightarrow 1_0$ state-to-state transition of NH_2D and that involve the various possible rotational states of H_2. From this figure, it appears that the transitions which are inelastic for H_2 are of lower magnitude than the elastic transition, by typically one or two orders of magnitude. Moreover, we find that the $J_2 = 2 \rightarrow 2$ transitions are larger than the $J_2 = 0 \rightarrow 0$ transitions. These conclusions apply to the whole set of transitions and were already reached for other molecular systems (see e.g. Dubernet et al. 2009; Daniel et al. 2010; Daniel, Dubernet & Grosjean 2011; Wiesenfeld & Faure 2013).

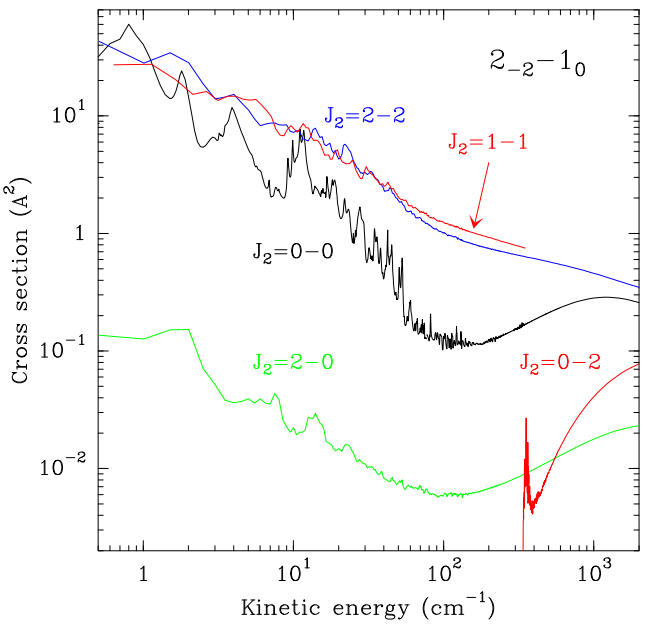

Figure 5. Cross-sections associated with the $2_{-2} \rightarrow 1_0$ NH_2D transition and corresponding to the various $J_2 \rightarrow J_2'$ H_2 transitions with para-H_2 either in its fundamental state ($J_2 = 0$) or first excited state ($J_2 = 2$). The cross-section with ortho-H_2 ($J_2 = 1-1$) is also indicated, for a reduced range of kinetic energies.

4 RATE COEFFICIENTS

The collisional de-excitation rate coefficients are calculated by averaging the cross-sections with a Maxwell–Boltzmann distribution that describes the distribution of velocity of the molecules in the gas (see e.g. equation 5 in Wiesenfeld et al. 2011). In Table 2, we give the de-excitation rate coefficients for levels up to $J_\tau = 2_2$, with $J_2 = 0 \rightarrow 0$, and for temperatures in the range $T = 5$–100 K. The way these rates are obtained is further discussed below. This table is directly comparable to table 7 of Machin & Roueff (2006) where the same quantities are given for the NH_2D/He system. The whole set of rate coefficients, with higher temperatures and with a more extended set of molecular levels, will be made available through the LAMDA (Schöier et al. 2005) and BASECOL (Dubernet et al. 2013) data bases.

4.1 Null CS cross-sections

As outlined in Section 3, the $J_\tau \rightarrow 0_0$ transitions where τ ranges from $\tau = -J + 1$ to $\tau = J - 1$ with a step of 2 are predicted to be equal to zero with the CS formalism. Using the available CC calculations, we are however able to calculate these rate coefficients for the transitions with $J \leq 3$ and up to 300 K with a reasonable accuracy (see Appendix). Since the current set of rate coefficients considers levels up to $J_\tau = 7_7$, it is necessary to estimate the rate coefficients for the transitions that connect the fundamental energy level to the levels with $J \geq 4$ which are predicted to be null with the CS formalism. To do so, we extrapolate the behaviour observed for the rates with levels such that $J < 4$ and derive the following expression :

$$R(J_{\tau_i} \rightarrow 0_0) = R(1_0 \rightarrow 0_0) \times \left(\frac{1}{1.35}\right)^{J-1} \times \left(\frac{1}{2.6}\right)^{i-1}$$
$$\text{with} \quad \tau_i = -J + 1 + 2 \times (i-1); \quad i \in [[1; n]]$$
$$\text{and} \quad n = E\left(\frac{2J+1}{2}\right). \qquad (1)$$

We can expect large errors of the corresponding rate coefficients, typically of a factor of 10 or higher, since this expression is established on the basis of a poor statistics. However, since the corresponding rate coefficients should play only a minor role in the pumping scheme, these uncertainties should not have noticeable consequences on the predicted line intensities. In any astrophysical application, this assumption should however be checked. For example, as was done in Daniel et al. (2013), the sensitivity of the line intensities to the corresponding rate coefficients can be assessed by considering randomly scaled values for these rates around their nominal value.

4.2 Rate coefficient accuracy

The accuracy of the current rate coefficients is limited by the following assumptions. A first source of error comes from the neglect of the inversion motion. However, we expect that this hypothesis should only have marginal effects on the rate coefficients, at least in comparison to the other sources of error. A second limitation comes from the fact that the PES was calculated for the equilibrium geometry of the NH_3 molecule. The PES was corrected for the displacement of the centre of mass between NH_3 and NH_2D, but the variation of the bond length from NH to ND was neglected. The effect introduced by taking into account the vibrationally averaged geometry of NH_2D, rather than taking the NH_3 internal

Table 2. De-excitation rate coefficients for NH_2D/H_2 ($J_2 = 0$–0) as a function of temperature and for NH_2D levels up to $J_\tau = 2_2$.

Transition	Rate coefficients ($cm^3\ s^{-1}$)					
	5K	10 K	25K	50 K	75K	100 K
$1_{0,1} \rightarrow 0_{0,0}$	1.24(−11)	1.17(−11)	9.58(−12)	6.86(−12)	5.41(−12)	4.58(−12)
$1_{1,1} \rightarrow 0_{0,0}$	2.00(−12)	2.06(−12)	1.62(−12)	9.69(−13)	6.45(−13)	4.66(−13)
$1_{1,1} \rightarrow 1_{0,1}$	1.17(−10)	1.20(−10)	1.16(−10)	1.06(−10)	1.02(−10)	1.01(−10)
$1_{1,0} \rightarrow 0_{0,0}$	5.56(−11)	6.65(−11)	7.22(−11)	6.93(−11)	6.79(−11)	6.80(−11)
$1_{1,0} \rightarrow 1_{0,1}$	1.46(−11)	1.38(−11)	9.61(−12)	6.05(−12)	4.56(−12)	3.89(−12)
$1_{1,0} \rightarrow 1_{1,1}$	1.55(−11)	1.52(−11)	1.16(−11)	8.35(−12)	6.79(−12)	5.90(−12)
$2_{0,2} \rightarrow 0_{0,0}$	9.34(−12)	6.89(−12)	4.68(−12)	3.24(−12)	2.62(−12)	2.29(−12)
$2_{0,2} \rightarrow 1_{0,1}$	2.76(−11)	2.73(−11)	2.70(−11)	2.61(−11)	2.58(−11)	2.60(−11)
$2_{0,2} \rightarrow 1_{1,1}$	1.79(−11)	1.42(−11)	9.32(−12)	5.85(−12)	4.39(−12)	3.70(−12)
$2_{0,2} \rightarrow 1_{1,0}$	2.28(−11)	2.17(−11)	1.84(−11)	1.47(−11)	1.30(−11)	1.22(−11)
$2_{1,2} \rightarrow 0_{0,0}$	2.00(−12)	1.89(−12)	1.29(−12)	7.45(−13)	4.94(−13)	3.58(−13)
$2_{1,2} \rightarrow 1_{0,1}$	7.80(−12)	7.14(−12)	5.16(−12)	3.42(−12)	2.58(−12)	2.14(−12)
$2_{1,2} \rightarrow 1_{1,1}$	2.69(−11)	2.71(−11)	2.60(−11)	2.48(−11)	2.46(−11)	2.47(−11)
$2_{1,2} \rightarrow 1_{1,0}$	1.25(−11)	1.05(−11)	6.61(−12)	3.85(−12)	2.76(−12)	2.27(−12)
$2_{1,2} \rightarrow 2_{0,2}$	9.57(−11)	9.58(−11)	1.05(−10)	1.09(−10)	1.11(−10)	1.13(−10)
$2_{1,1} \rightarrow 0_{0,0}$	5.35(−12)	4.60(−12)	3.43(−12)	2.50(−12)	2.14(−12)	2.04(−12)
$2_{1,1} \rightarrow 1_{0,1}$	5.38(−11)	5.58(−11)	6.03(−11)	6.10(−11)	6.13(−11)	6.20(−11)
$2_{1,1} \rightarrow 1_{1,1}$	2.90(−11)	3.06(−11)	2.92(−11)	2.44(−11)	2.10(−11)	1.88(−11)
$2_{1,1} \rightarrow 1_{1,0}$	8.99(−12)	7.69(−12)	5.67(−12)	4.23(−12)	3.57(−12)	3.22(−12)
$2_{1,1} \rightarrow 2_{0,2}$	1.48(−11)	1.47(−11)	1.16(−11)	8.26(−12)	6.95(−12)	6.54(−12)
$2_{1,1} \rightarrow 2_{1,2}$	2.35(−11)	2.37(−11)	2.33(−11)	2.26(−11)	2.25(−11)	2.28(−11)
$2_{2,1} \rightarrow 0_{0,0}$	8.19(−13)	6.91(−13)	4.63(−13)	2.76(−13)	1.87(−13)	1.37(−13)
$2_{2,1} \rightarrow 1_{0,1}$	2.36(−11)	2.51(−11)	2.60(−11)	2.27(−11)	1.99(−11)	1.81(−11)
$2_{2,1} \rightarrow 1_{1,1}$	5.44(−11)	5.61(−11)	6.01(−11)	6.14(−11)	6.23(−11)	6.35(−11)
$2_{2,1} \rightarrow 1_{1,0}$	3.14(−12)	2.78(−12)	2.10(−12)	1.48(−12)	1.21(−12)	1.10(−12)
$2_{2,1} \rightarrow 2_{0,2}$	3.05(−11)	2.54(−11)	1.97(−11)	1.66(−11)	1.55(−11)	1.50(−11)
$2_{2,1} \rightarrow 2_{1,2}$	2.33(−11)	1.91(−11)	1.31(−11)	9.46(−12)	8.31(−12)	8.10(−12)
$2_{2,1} \rightarrow 2_{1,1}$	3.16(−11)	3.87(−11)	4.37(−11)	4.23(−11)	4.12(−11)	4.09(−11)
$2_{2,0} \rightarrow 0_{0,0}$	1.63(−11)	1.58(−11)	1.43(−11)	1.21(−11)	1.06(−11)	9.73(−12)
$2_{2,0} \rightarrow 1_{0,1}$	6.02(−12)	5.20(−12)	4.03(−12)	3.11(−12)	2.68(−12)	2.46(−12)
$2_{2,0} \rightarrow 1_{1,1}$	3.85(−12)	3.24(−12)	2.46(−12)	1.87(−12)	1.63(−12)	1.57(−12)
$2_{2,0} \rightarrow 1_{1,0}$	7.38(−11)	7.42(−11)	7.48(−11)	7.43(−11)	7.48(−11)	7.60(−11)
$2_{2,0} \rightarrow 2_{0,2}$	2.24(−11)	1.98(−11)	1.57(−11)	1.20(−11)	1.00(−11)	8.82(−12)
$2_{2,0} \rightarrow 2_{1,2}$	1.57(−11)	1.72(−11)	1.88(−11)	1.85(−11)	1.82(−11)	1.82(−11)
$2_{2,0} \rightarrow 2_{1,1}$	1.33(−11)	1.25(−11)	8.88(−12)	5.83(−12)	4.48(−12)	3.84(−12)
$2_{2,0} \rightarrow 2_{2,1}$	9.50(−12)	8.68(−12)	9.44(−12)	9.41(−12)	9.05(−12)	8.78(−12)

geometry, can lead to noticeable effects. Such a modification was tested for D_2O by Scribano et al. (2010), where rate coefficients for this isotopologue were calculated using the H_2O internal geometry. Differences of the order of 30 per cent were found, and we might expect differences of the same order for NH_2D. Finally, a third source of error resides in the use of the CS formalism at high temperatures. As described in Section 3 and in Appendix , the CS calculations were scaled according to some reference calculations performed with the CC formalism. However, an inherent limitation of this procedure comes from the uncertainty introduced by the scattering of the ratios which are due to the resonances. Moreover, the ratios were extrapolated at the highest energies. Finally, for the transitions that involve energy levels higher than the 4_2 level, we directly computed the rate coefficients using the original CS cross-sections.

In order to have an estimate of the error introduced in the rate coefficients due to the use of the CS formalism, we compared the rate coefficients calculated with the scaled CS cross-sections [noted $R^s(i \rightarrow j)$] to the rates calculated with the unscaled cross-sections [noted $R^u(i \rightarrow j)$]. The minimum and maximum values of the ratios $R^s(i \rightarrow j)/R^u(i \rightarrow j)$ found in the range $T = 5$–300 K are reported in the upper panel of Fig. 6 for all the de-excitation transitions up to $J_\tau = 3_3$. In the lower panel of this figure, we report the same quantities, but for levels up to $J_\tau = 4_2$ and for the temperature range $T = 50-300$ K. From this figure, it can be seen that for the transitions that involve levels up to the 3_{-1} ($E \sim 75$ cm^{-1}), the scaled and unscaled rate coefficients differ by less than 20 per cent (upper panel). On the other hand, for higher energy levels, the differences can be as high as a factor of ∼2 but most of the transitions (93 per cent of the 253 transitions considered here) show differences below a factor of 1.3. We note that the reason why the lowest energy levels are less affected by the scaling of the cross-sections comes from the fact that a larger part of the grid corresponds to CC calculations for these levels. Finally, given the variations observed for the $R^s(i \rightarrow j)/R^u(i \rightarrow j)$ ratios, we can expect that the transitions that involve an energy level above $J_\tau = 4_2$ will have a typical accuracy of 30 per cent, since these transitions are directly calculated from the CS cross-sections.

To summarize the previous considerations, considering the current PES, we expect that the current rate coefficients will be accurate within 5 per cent for the transitions up to $J_\tau = 4_2$. For higher energy

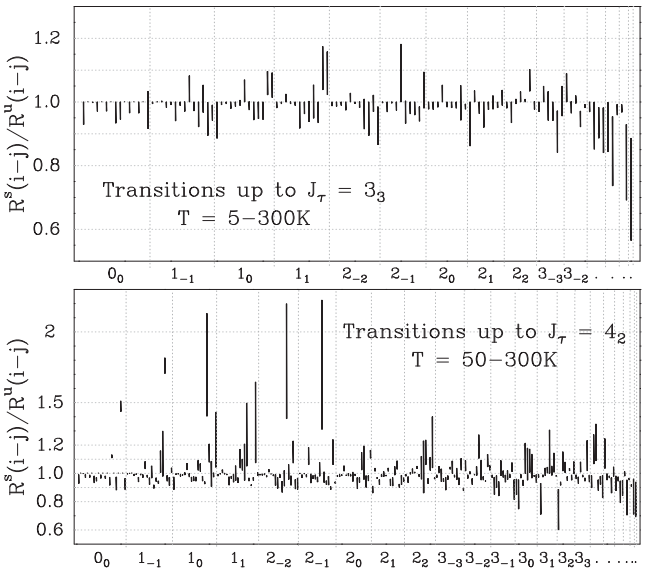

Figure 6. Upper panel: range of the variations found in the temperature range $T = 5$–300 K, between the scaled and unscaled collisional rate coefficients for the levels up to $J_\tau = 3_3$. The x-axis gives the final level of the de-excitation collisional rate coefficient. For each final level, the variations are given for all the de-excitation rates, ordered by increasing value of the upper energy level state. Lower panel: same as the upper panel but for the transitions which consider levels up to $J_\tau = 4_2$ and for the temperature range $T = 50$–300 K.

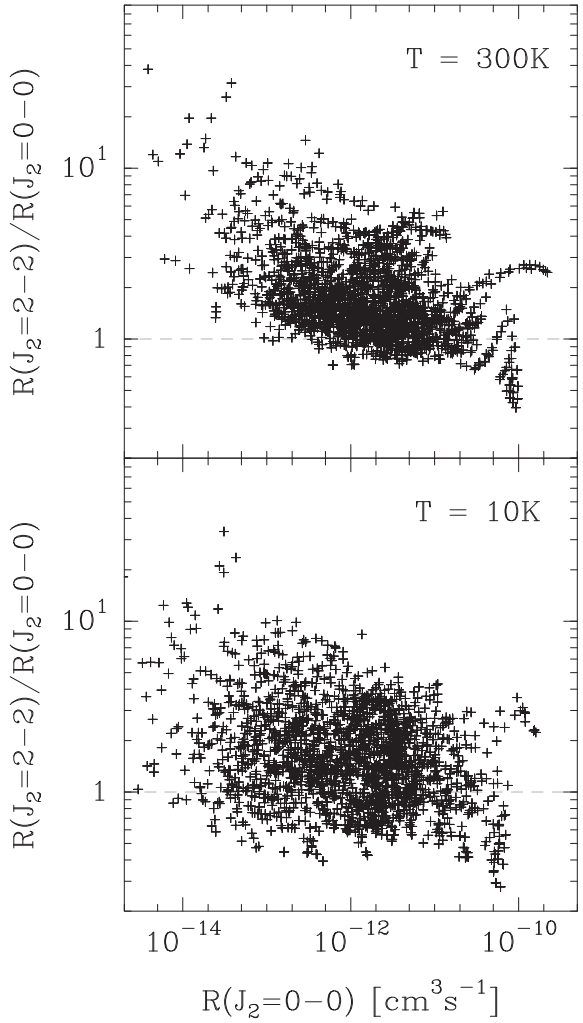

Figure 7. Ratio of the rate coefficients associated with the $J_2 = 2 \rightarrow 2$ over the rate with $J_2 = 0 \rightarrow 0$, as a function of the magnitude of the rate coefficients associated with the para-H_2 fundamental state. The ratios are given at $T = 10$ K (lower panel) and $T = 300$ K (upper panel).

levels, the accuracy should be of the order of 30 per cent. This holds true for all transitions except for the $J_\tau \rightarrow 0_0$ transitions, where τ ranges from $\tau = -J + 1$ to $\tau = J - 1$ with a step of 2. For these transitions and for the levels such that $J < 4$, the rates should be accurate to within 30 per cent. For higher levels, i.e. with $J \geq 4$, we can expect an error up to a factor of 10 in the rate coefficients. Most importantly, a dominant source of error resides in the fact that the PES was calculated for a molecular geometry which corresponds to the NH_3 internal geometry. Thus, we might expect an additional 30 per cent uncertainty on the rate coefficients (Scribano et al. 2010).

4.3 Thermalized rate coefficients

The previous discussion dealt with rate coefficients where para-H_2 was restricted to its fundamental state $J_2 = 0$. Such rate coefficients are enough to tackle astrophysical applications that deal with cold media (i.e. $T < 50$ K). However, at higher gas temperatures, we expect a larger fraction of the H_2 molecules in excited states ($J_2 > 0$). As discussed in Section 3, the cross-sections with $J_2 = 2 \rightarrow 2$ are of larger magnitude than the cross-sections associated with the $J_2 = 0 \rightarrow 0$ transitions. This is shown in Fig. 7 where we represent the ratio of the rate coefficients with $J_2 = 2 \rightarrow 2$ to that with $J_2 = 0 \rightarrow 0$, for temperatures of 10 and 300 K. On average, the rate coefficients with $J_2 = 2 \rightarrow 2$ are of larger magnitude, with an average ratio slightly increasing from 2 to 2.4 with temperature increasing from 10 to 300 K. However, as can be seen from Fig. 7, the variation in magnitude of the rate coefficient depends on the absolute magnitude of the rate, the variation being larger for the rates of lower magnitude. Moreover, as seen in Fig. 7, there is a large scatter of the ratios. Thus, by varying the relative populations of the fundamental and first H_2 excited states, the number of collisionally induced events will be modified accordingly, i.e. the number of events becomes larger with increasing the fractional abundance of the first excited state. To take this effect into account, we define thermalized rate coefficients, following the definition given in Dubernet et al. (2009, equation 4).

Finally, we stress that in hot media, the relevant collisional partner will be ortho-H_2 rather than para-H_2 and in such a case, it should be necessary to calculate the corresponding rate coefficients. However, in the case of the H_2O/H_2 collisional system, it was found that the effective rate coefficients for $J_2 = 2$ and $J_2 = 1$ agree within ∼30 per cent (Dubernet et al. 2009; Daniel et al. 2010, 2011). More generally, these studies showed that apart from the rate coefficients in $J_2 = 0$, all the effective rate coefficients with $J_2 > 0$ are qualitatively similar, independently of the H_2 symmetry. As a consequence, in astrophysical applications, the thermalized rate coefficients with ortho-H_2 or para-H_2 lead to similar line intensities at high temperatures (Daniel et al. 2012). To conclude, this means that in principle, the rate coefficients with $J_2 = 2 \rightarrow 2$ can serve as a template to emulate the rate coefficients of ortho-H_2 ($J_2 = 1 \rightarrow 1$). We checked this assumption by performing a few calculations with ortho-H_2 as a collisional partner. In Fig. 5, we compare the cross-sections of the $2_{-2}-1_0$ transition associated with either $J_2 = 2 \rightarrow 2$ or $J_2 = 1 \rightarrow 1$.

It can be seen that these two cross-sections are qualitatively similar for the energy range considered here. Such agreement is also found on a more general basis. Considering a statistics over the $i \rightarrow j$ transitions, we obtained that, whatever the energy, the mean value μ of the ratios $\sigma_{ij}(2 \rightarrow 2)/\sigma_{ij}(1 \rightarrow 1)$ is $\mu \sim 1$, with a standard deviation σ that varies with energy in the range $\sigma = 0.15-0.30$. For each energy, ∼70 per cent of the transitions vary by less than 1σ around μ and ∼95 per cent of the transitions are within 2σ. Thus, this confirms that the rate coefficients in $J_2 = 2 \rightarrow 2$ are a good approximation for the ortho-H_2 rate coefficients.

5 DISCUSSION

Prior to this work, the only available rate coefficients for NH_2D were calculated with He as a collisional partner. Rate coefficients with He are often used as a template to estimate the rate coefficients with H_2. However, for many molecules, large differences exist and the rates do not scale accordingly to the factor ∼1.4 deduced from the difference in the reduced masses of the two colliding systems. Concerning the deuterated isotopologues of ammonia, such a conclusion was already reached for ND_2H. Indeed, for this particular isotopologue, the He and H_2 rate coefficients were found to vary by factors in the range 3–30 (Machin & Roueff 2007; Wiesenfeld et al. 2011). In Fig. 8, we give the ratios of the current NH_2D/H_2 rate coefficients with the rates calculated with He (Machin & Roueff 2006), as a function of the magnitude of the H_2 rate coefficients and for temperatures of $T = 10$ and 100 K. The comparison concerns the transitions that involve levels up to $J_\tau = 2_2$ (the highest level considered in Machin & Roueff 2006). From this figure, it appears that the H_2 and He rate coefficients show large variations, as expected from the previous studies of ND_2H. At $T = 10$ K, the ratios are in the range 1–100. Moreover, it appears that the largest differences are also found for the largest rate coefficients. At higher temperatures, we obtain the same trend except that the range of variations is reduced. For example, at $T = 100$ K, the ratios for the lowest rate coefficients are around 1, while they are around 20 for the highest rates.

Finally, one may wonder if it is possible to infer the rate coefficients of singly deuterated ammonia from the rates of doubly deuterated ammonia, or vice versa. A direct comparison of the current rates with the values reported by Wiesenfeld et al. (2011) for ND_2H/H_2 would not be totally meaningful, at least quantitatively, since in the latter study, the dynamical calculations were performed with a $J_2 = 0$ basis for H_2. As discussed in Section 3, considering a $J_2 = 0, 2$ basis for H_2 can induce variations as large as a factor of ∼7, and the magnitudes of the effects are presumably similar for ND_2H. We thus performed a few additional calculations for the ND_2H/H_2 system. These calculations are similar to the ones presented in Wiesenfeld et al. (2011) except for the H_2 basis which is now set to $J_2 = 0, 2$. In Fig. 9, we compare the cross-sections of NH_2D and ND_2H for the six de-excitation transitions possible when considering the levels up to $J_\tau = 1_1$. From this figure, it appears that on the average, the cross-sections are of the same order of magnitude for the two colliding systems. The differences are definitely lower than those found with He as a collisional partner. However, above 5 cm^{-1}, differences of a factor of ∼3 or higher may occur when considering individual transitions. This implies that a dedicated calculation is necessary to infer accurate rate coefficients for a particular isotopologue. Furthermore, given the differences obtained between the rate coefficients calculated with H_2 or He, the current comparison shows that in the absence of a dedicated calculation, the rate coefficients of a deuterated isotopologue should be preferentially taken from another isotopologue with the same symmetry rather than scaled from the He rates. As an example, to emulate the CD_2H/H_2 rate coefficients, it should be more accurate to take the CH_2D/H_2 rate coefficients than the CD_2H/He one.

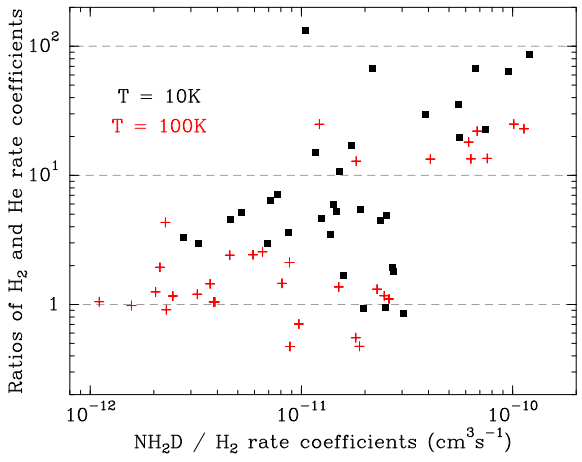

Figure 8. Comparison between the current NH_2D/H_2 rate coefficients with the rates calculated with He as a collisional partner (Machin & Roueff 2006).

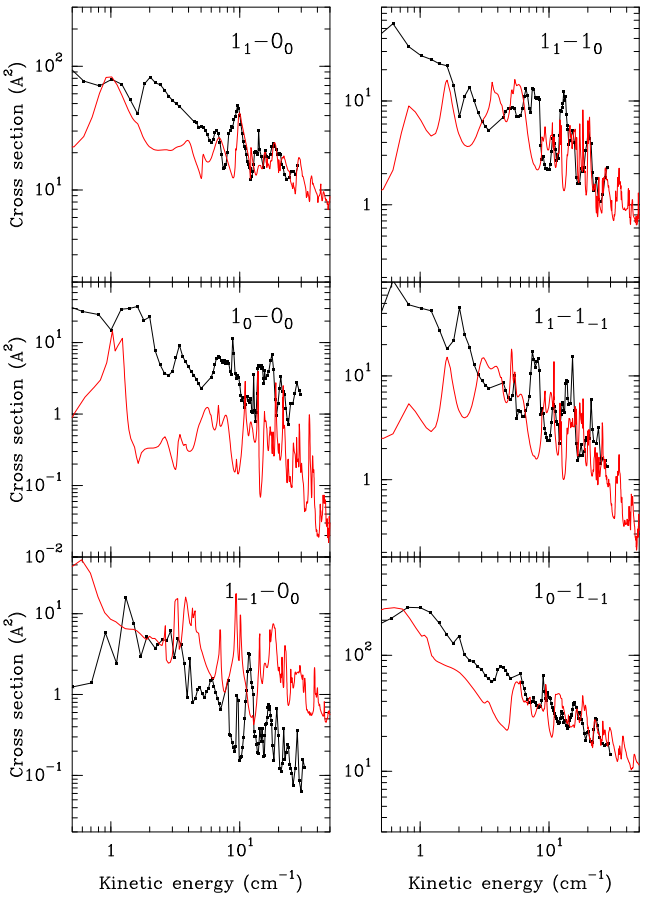

Figure 9. Comparison between the NH_2D (red) and ND_2H (black) cross-sections calculated with H_2 ($J_2 = 0, 2$).

6 CONCLUSIONS

We reported the calculation of collisional rate coefficients for the NH_2D/H_2 system for NH_2D rotational energy levels up to $J_\tau = 7_7$ ($E \sim 735$ K) and for temperatures in the range $T = 5$–300 K. These rate coefficients will be made available through the BASECOL (Dubernet et al. 2013) and LAMDA (Schöier et al. 2005) data bases. The current rate coefficients were calculated by adapting the NH_3/H_2 PES presented in Maret et al. (2009). The dynamical calculations were performed at the CC level at low total energy ($E < 110$ cm^{-1}) and with the CS formalism at higher energies. For the levels up to $J_\tau = 4_2$, the CS cross-sections were scaled according to some reference points performed with the accurate CC formalism. For these transitions and for the current PES, the accuracy of the rate coefficients is expected to be of the order of 5 per cent. For higher energy levels, the accuracy is limited by the use of the CS formalism, and the corresponding rate coefficients are expected to be accurate within 30 per cent. These uncertainties concern all the transitions except the $J_\tau \rightarrow 0_0$ transitions with J_τ varying from $-J+1$ to $J-1$ in a step of 2. For the latter transitions, we expect the rate coefficients to be accurate within 30 per cent for the levels with $J \leq 3$ while for the levels such that $J \geq 4$, the rate coefficients have uncertainties of the order of a factor of 10. We note that these errors only consider the accuracy of the dynamical calculations and do not take into account other sources of uncertainty like the accuracy of the PES or the neglecting of the inversion motion. For what concerns the PES, we might expect an additional 30 per cent uncertainty on the rate coefficients, which is to be added in quadrature to the previously mentioned uncertainties, since the current PES was calculated for an internal geometry suitable to NH_3.

ACKNOWLEDGEMENTS

All (or most of) the computations presented in this paper were performed using the CIMENT infrastructure (https://ciment.ujf-grenoble.fr), which is supported by the Rhône–Alpes region (GRANT CPER07_13 CIRA: http://www.ci-ra.org). DL support for this work was provided by NASA (*Herschel* OT funding) through an award issued by JPL/Caltech. This work has been supported by the Agence Nationale de la Recherche (ANR-HYDRIDES), contract ANR-12-BS05-0011-01 and by the CNRS national programme 'Physico-Chimie du Milieu Interstellaire'.

REFERENCES

Busquet G., Palau A., Estalella R., Girart J. M., Sánchez-Monge Á., Viti S., Ho P. T. P., Zhang Q., 2010, A&A, 517, L6
Cohen E. A., Pickett H. M., 1982, J. Mol. Spectrosc., 93, 83
Coudert L. H., Roueff E., 2006, A&A, 449, 855
Coudert L., Valentin A., Henry L., 1986, J. Mol. Spectrosc., 120, 185
Daniel F., Dubernet M.-L., Pacaud F., Grosjean A., 2010, A&A, 517, A13
Daniel F., Dubernet M.-L., Grosjean A., 2011, A&A, 536, A76
Daniel F., Goicoechea J. R., Cernicharo J., Dubernet M.-L., Faure A., 2012, A&A, 547, A81
Daniel F. et al., 2013, A&A, 560, A3
Dubernet M.-L., Daniel F., Grosjean A., Lin C. Y., 2009, A&A, 497, 911
Dubernet M.-L. et al., 2013, A&A, 553, A50
Faure A., Valiron P., Wernli M., Wiesenfeld L., Rist C., Noga J., Tennyson J., 2005, J. Chem. Phys., 122, 221102
Hatchell J., 2003, A&A, 403, L25
Heil T. G., Kouri D. J., Green S., 1978, J. Chem. Phys., 68, 2562
Huber K. P., Herzberg G., 1979, Molecular Spectra and Molecular Structure IV. Constants of Diatomic Molecules. Van Nostrand-Reinhold, New York
McGuire P., Kouri D. J., 1974, J. Chem. Phys., 60, 2488
Machin L., Roueff E., 2006, A&A, 460, 953
Machin L., Roueff E., 2007, A&A, 465, 647
Maret S., Faure A., Scifoni E., Wiesenfeld L., 2009, MNRAS, 399, 425
Müller H. S. P., Thorwirth S., Roth D. A., Winnewisser G., 2001, A&A, 370, L49
Neill J. L., Crockett N. R., Bergin E. A., Pearson J. C., Xu L.-H., 2013, ApJ, 777, 85
Olberg M., Bester M., Rau G., Pauls T., Winnewisser G., Johansson L. E. B., Hjalmarson A., 1985, A&A, 142, L1
Pillai T., Wyrowski F., Hatchell J., Gibb A. G., Thompson M. A., 2007, A&A, 467, 207
Rist C., Faure A., 2011, J. Math. Chem., 50, 588
Rodriguez Kuiper E. N., Kuiper T. B. H., Zuckerman B., 1978, ApJ, 219, L49
Roueff E., Lis D. C., van der Tak F. F. S., Gerin M., Goldsmith P. F., 2005, A&A, 438, 585
Saito S., Ozeki H., Ohishi M., Yamamoto S., 2000, ApJ, 535, 227
Schöier F. L., van der Tak F. F. S., van Dishoeck E. F., Black J. H., 2005, A&A, 432, 369
Scribano Y., Faure A., Wiesenfeld L., 2010, J. Chem. Phys., 133, 231105
Shah R. Y., Wootten A., 2001, ApJ, 554, 933
Tiné S., Roueff E., Falgarone E., Gerin M., Pineau des Forêts G., 2000, A&A, 356, 1039
Turner B. E., Zuckerman B., Morris M., Palmer P., 1978, ApJ, 219, L43
Walmsley C. M., Hermsen W., Henkel C., Mauersberger R., Wilson T. L., 1987, A&A, 172, 311
Wiesenfeld L., Faure A., 2013, MNRAS, 432, 2573
Wiesenfeld L., Scifoni E., Faure A., Roueff E., 2011, MNRAS, 413, 509

APPENDIX A: SCALING OF THE CS CROSS-SECTIONS

In order to obtain accurate cross-sections, we scaled the CS cross-sections according to a few calculations performed with the CC formalism. These CC calculations were performed for total energies in the range $110 < E < 250$ cm^{-1}. The ratio of the CC to CS cross-sections is reported in Fig. A2 for a few transitions. In order to correct the CS cross-sections, we performed an analytical fit of the ratio and to that purpose, we used two fitting functions

$$f(E) = \sum_{i \in \{1,3\}} a_i \, E^{i-2} \tag{A1}$$

$$g(E) = \sum_{i \in \{1,3\}} a_i \, E^{i-2} + a_4 \, \mathrm{e}^{-0.1\,E}, \tag{A2}$$

where E corresponds to the total energy. The latter functional form was used to reproduce the oscillating behaviour seen in some transitions (like e.g. the 2_{-1}–1_{-1}, 3_0–1_{-1} or 3_0–2_0 transition shown in Fig. A2). The choice of the functional form is made automatically, and for a given transition the function $g(E)$ is selected as soon as the χ^2 obtained with this function is lower by at least a factor of 3 by comparison to the χ^2 obtained with the function $f(E)$.

Considering the behaviour of the ratios reported in Fig. A2, it appears that the ratios depend on the total energy and, in most cases, tend to get close to 1 at the highest energies. Since we are interested in scaling the cross-sections up to $\sim$3000 cm^{-1}, we extrapolate the ratios at energies higher than 250 cm^{-1}. To do so, we proceed as follows. We first fit a linear function using the ratios obtained at the highest energies. This leads to two possible behaviours depending on the energy where the resulting line crosses the $y = 1$ axis (denoted by x_0 in what follows). In the first case, $x_0 > 250$ cm^{-1}, and we then use the $f(E)$ functional form to extrapolate the ratios at high energy. In the fitting procedure, we put as an additional constraint

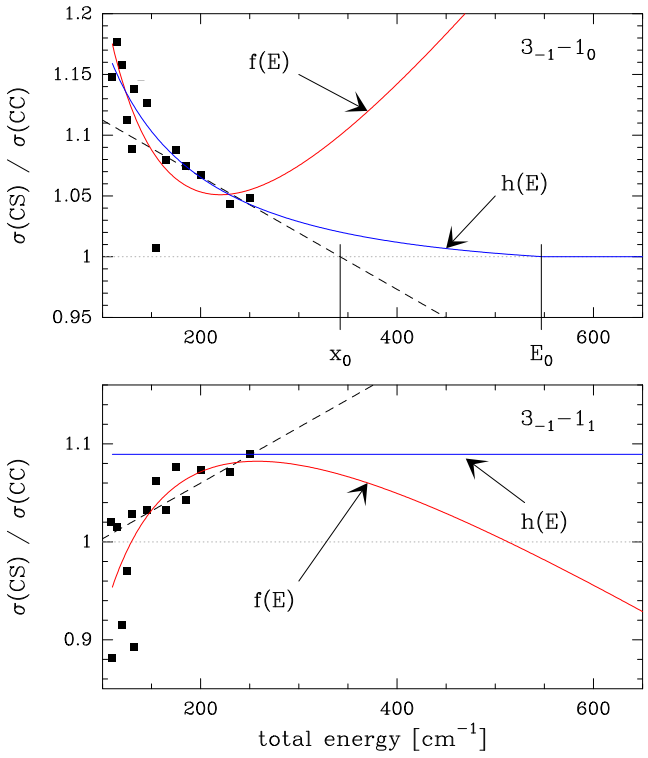

Figure A1. Extrapolation of the CS/CC ratios (see the text for details).

that the ratio is 1 at $E_0 = 1.5\,x_0$. Above E_0, the ratio is set to 1. In the second case, $x_0 < 250$ cm^{-1}. In this case, we fix the ratio above 250 cm^{-1} and keep the value obtained at the latest energy. This extrapolation procedure thus gives the function $h(E)$. These two cases are illustrated in Fig. A1 where we show the result of the fitting procedure for the $3_{-1}-1_0$ transition (case 1) and $3_{-1}-1_{-1}$ transition (case 2).

Finally, to ensure the continuity between the two fitting functions, we define the function $\phi(E)$, which gives the correction of the CS cross-sections in the range $110 < E < 3000$ cm^{-1}:

$$\phi(E) = f(E) \text{ or } g(E) \quad \text{if} \quad E < 170\,\text{cm}^{-1} \tag{A3}$$

$$\phi(E) = (1-w)\,f(E) + w\,h(E) \quad \text{if} \quad 170 < E < 250\,\text{cm}^{-1} \tag{A4}$$

$$\phi(E) = h(E) \quad \text{if} \quad E > 250\,\text{cm}^{-1}, \tag{A5}$$

where w is a weighting function that varies linearly between 0 and 1 in the range $170 < E < 250$ cm^{-1}. The resulting fit is shown in Fig. A2 for a few transitions which are characteristic of the behaviour observed on the whole sample of transitions.

APPENDIX B: NULL CS CROSS-SECTIONS

As outlined in Sections 3 and 4, the $J_\tau \rightarrow 0_0$ transitions where τ ranges from $\tau = -J + 1$ to $\tau = J - 1$ in a step of 2 are predicted to be equal to zero with the CS formalism. Since we performed CC calculations below 110 cm^{-1} with some additional points between 110 and 250 cm^{-1}, we are however able to calculate the rate coefficients for a few of these transitions and up to 300 K, despite the lack of calculated points above 250 cm^{-1}. This is due to the fact that the corresponding cross-sections decrease sharply with the kinetic energy. This is illustrated in Fig. B1 for the $1_0 \rightarrow 0_0$, $2_1 \rightarrow 0_0$ and $3_2 \rightarrow 0_0$ transitions. The upper panel in this figure shows the available CC points as well as two possible extrapolations of the cross-sections above 250 cm^{-1}. The first extrapolation is obtained using a polynomial fit of the CC cross-sections (plain curves) while

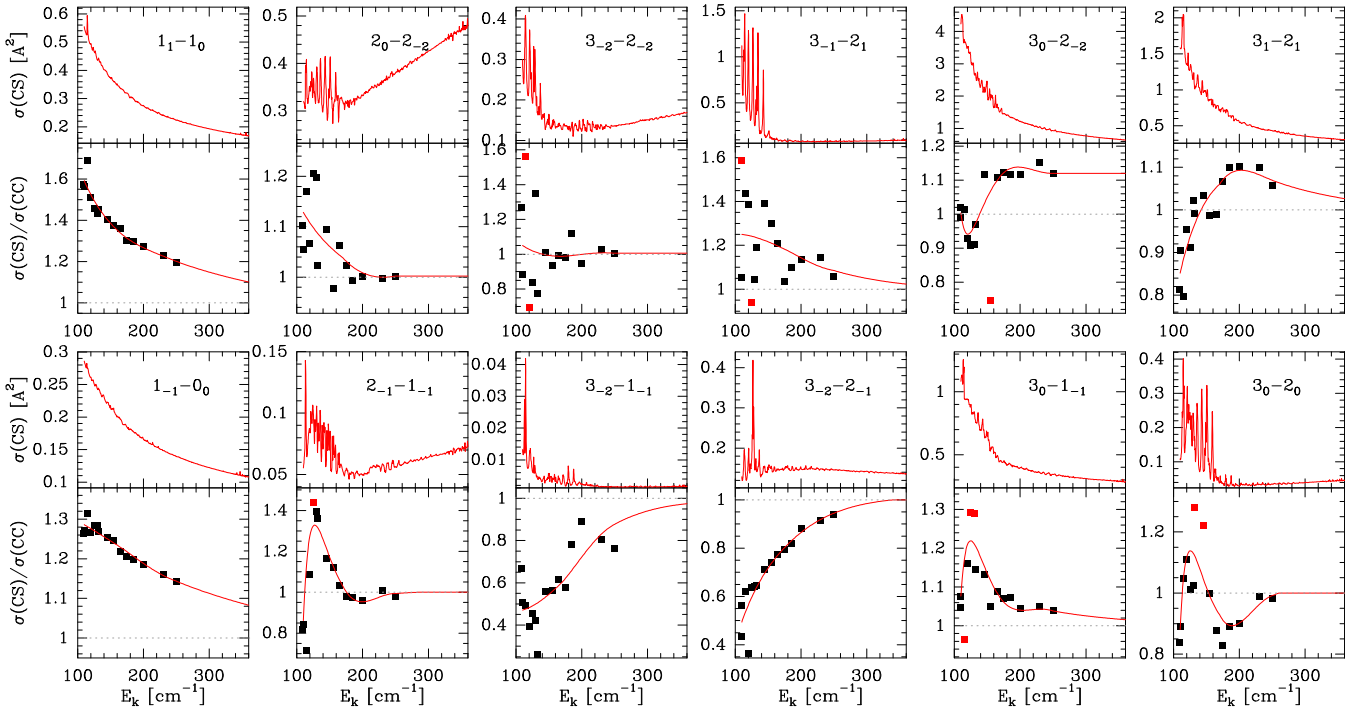

Figure A2. In each panel, the upper plot shows the unscaled CS cross-sections in Å^2. In the lower plot, the black dots correspond to the ratios of the CC to CS cross-sections and the red curves show a fit of these ratios.

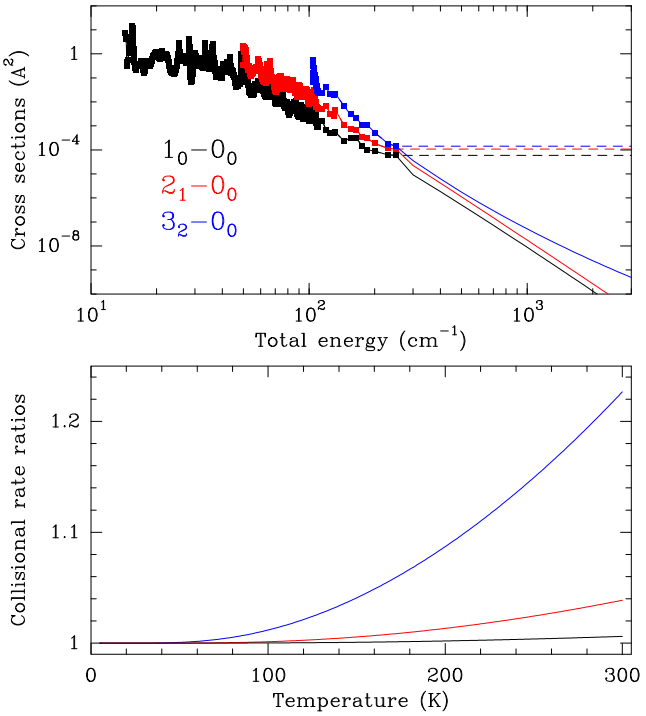

Figure B1. The upper panel gives the CC cross-sections of the $1_0 \rightarrow 0_0$, $2_1 \rightarrow 0_0$ and $3_2 \rightarrow 0_0$ transitions as a function of the total energy. The plain curves correspond to an extrapolation of these cross-sections based on a polynomial fit. The dashed curves, which assume constant values above 250 cm^{-1}, would correspond to an upper limit of the cross-sections at high energies. The lower panel gives the ratios of the rate coefficients obtained with the two extrapolations considered in the upper panel (same colour code).

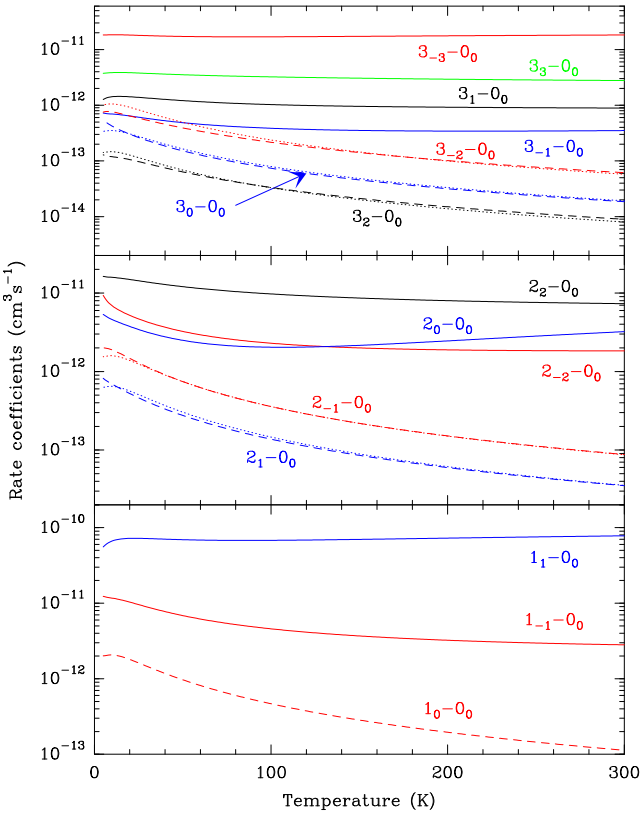

Figure B2. Rate coefficients for the transitions connecting the levels from $J = 1$ (lower panel), $J = 2$ (middle panel) and $J = 3$ (upper panel) to the fundamental energy level. The transitions for which the CS formalism predicts non-null rate coefficients are indicated as plain curves. For the other transitions for which the CS formalism predicts null cross-sections, the dashed curves correspond to the rate coefficients calculated from the available CC points. In the latter case, for the transitions from $J = 2$ and $J = 3$, we also show rate coefficients which are scaled from the $1_0 \rightarrow 0_0$ transition (dotted curves).

the second way of extrapolating takes a constant value for the cross-sections above a total energy of 250 cm^{-1} (dashed curves). These two limiting cases seem reasonable in view of the overall behaviour of the cross-sections shown in Fig. 4. Using these two extrapolations, we then calculated the corresponding rate coefficients for $T = 5{-}300$ K and their ratios are indicated in the bottom panel of Fig. B1. It can be seen that for these transitions, the rate coefficients are identical, within 2 per cent, below $T = 100$ K. For larger temperatures, we obtain larger differences, the discrepancies being the highest at 300 K. However, the variations are always below 25 per cent and this conclusion holds true for the seven transitions that consider the levels below the $J_\tau = 3_2$ level.

Since the current set of rate coefficients considers levels up to $J = 7$, it is necessary to complete the current set. To do so, we extrapolate the behaviour observed for the rates with levels such that $J < 4$. In Fig. B2, we show the various rate coefficients calculated for the levels up to $J_\tau = 3_3$. First, as can be seen in Fig. 4, the rate coefficients associated with the transitions predicted to be null with the CS formalism are systematically of lower magnitude than the rates of the other transitions. Thus, they should presumably play a minor role in the radiative transfer calculations. Moreover, all these transitions show a similar trend with temperature and are roughly proportional. As a consequence, it is possible to mimic the rate of a given transition using the rate coefficient, for example, of the $1_0 \rightarrow 0_0$ transition. The dotted curves in Fig. B2, for the transitions from $J = 2$ and $J = 3$, are approximated in this way by using the analytical expressions:

$$R(2_{-1} \rightarrow 0_0) = R(1_0 \rightarrow 0_0) \times \left(\frac{1}{1.3}\right) \tag{B1}$$

$$R(2_1 \rightarrow 0_0) = R(1_0 \rightarrow 0_0) \times \left(\frac{1}{1.3}\right) \times \frac{1}{2.45} \tag{B2}$$

$$R(3_{-2} \rightarrow 0_0) = R(1_0 \rightarrow 0_0) \times \left(\frac{1}{1.4}\right)^2 \tag{B3}$$

$$R(3_0 \rightarrow 0_0) = R(1_0 \rightarrow 0_0) \times \left(\frac{1}{1.4}\right)^2 \times \frac{1}{3} \tag{B4}$$

$$R(3_2 \rightarrow 0_0) = R(1_0 \rightarrow 0_0) \times \left(\frac{1}{1.4}\right)^2 \times \frac{1}{3} \times \frac{1}{2.4}. \tag{B5}$$

It can be seen in Fig. B2 that this simple scaling of the $1_0 \rightarrow 0_0$ rate coefficient can reproduce qualitatively the rate coefficients directly obtained from the integration of the cross-sections (dashed curves). From this trend, we can generalize the above equations, and the resulting expression corresponds to equation (1) of Section 4.

This paper has been typeset from a TEX/LATEX file prepared by the author.